

Stress-strain model of lower corroded steel plates of normal strength for fitness-for-purpose analyses

Krzysztof Wołoszyk^a, Yordan Garbatov^{b, 1}, Paweł Kłosowski^c

^a *Institute of Naval Architecture and Ocean Engineering, Gdansk University of Technology,
G. Narutowicza 11/12 st., 80-233 Gdansk, Poland*

^b *Centre for Marine Technology and Ocean Engineering (CENTEC), Instituto Superior Técnico,
Universidade de Lisboa, Avenida Rovisco Pais 1049-001 Lisboa, Portugal*

^c *Faculty of Civil and Environmental Engineering, Gdansk University of Technology,
G. Narutowicza 11/12 st., 80-233 Gdansk, Poland*

Abstract

This study investigates the mechanical properties of specimens made of normal strength steel subjected to lower marine immersed corrosion degradation levels (below 25 %). The specimens were corroded in laboratory conditions, and only natural factors were controlled to raise the corrosion rate (reaching the level of 1 mm/year). Three different thicknesses of plates made of normal strength of shipbuilding steel are investigated (between 5 mm and 8 mm). The standard tensile tests are performed for estimating the stress-strain behaviour of corroded specimens. Non-corroded specimens were tested to establish the initial mechanical properties and uncertainty level as a reference. Further, the corroded specimens were tested too. Based on that, the changes in mechanical properties (i.e. yield stress, Young modulus, ultimate tensile stress and total elongation) were analysed. It was found, that for degradation level reaching 25%, approx. 10% reduction of yield stress was observed. A new parameter, defining the area reduction, was established as more closely related to the mechanical properties deterioration than the commonly used a mean degradation level. The bilinear stress-strain model of corroded steel plates was proposed for the fitness-for-purpose analyses in the structural integrity assessment.

Keywords: corrosion, mechanical properties, marine environment, fitness-for-purpose

¹ Corresponding author e-mail: yordan.garbatov@tecnico.ulisboa.pt; Telf (351) 21 841 7907

29 1 Introduction

30 Ships and offshore structures operating at sea are subjected to a highly corrosive environment. The
31 non-uniform corrosion degradation is a factor that can significantly affect the load-carrying capacity of
32 different structural members [1–4], mainly due to cross-sectional area reduction and decrease of
33 mechanical properties. One can identify the most common types of corrosion, like pitting and general
34 corrosion [5]. The examples of these two corrosion types that could be found in ship structures are
35 distinguished in industrial guidelines, such as [6], where examples of real corroded structures are
36 presented (see Figure 1). Pitting corrosion is a very localised degradation phenomena that results in
37 the creation of small holes in the metal. On the other hand, general corrosion is spread within the
38 entire surface, but degradation level is non-uniform within the structural components. These two types
39 of corrosion need to be treated separately in terms of modelling and analysis.



40

41 Figure 1. The comparison between general (left) and pitting corrosion (right) [6].

42 The corrosion causes not only general thickness loss but also a reduction of mechanical properties.
43 This, in consequence, could result in a collapse of various structural components or even entire
44 structure. Thus, the investigation of this phenomenon is of crucial importance from the safety point of
45 view. Recently, more studies related to that problem were performed. When dealing with ship
46 structures, most important are flat specimens, taken from thin-walled structural elements. One of the
47 first attempts to investigate the mechanical properties of corroded steel specimens with different
48 corrosion severity were made by Garbatov et al. [7]. In this case, the typical coupon specimens were
49 taken from a corroded box girder [8], which was corroded in seawater with the additional electric
50 current applied. The corrosion degradation level of specimens was very high in that case and varied
51 between 25% up to 75%. It was found that all mechanical properties were reduced, i.e. yield strength,
52 Young's modulus, ultimate tensile stress and total elongation. The observed reduction of yield stress
53 was around 15% for degradation level of 50%, and mean thickness after corrosion was taken as the
54 reference to calculate the mechanical properties.

55 The mechanical properties of corroded flat-bar specimens subjected to atmospheric corrosion were
56 investigated too. Samples taken from truss corroded in natural atmospheric conditions with different
57 thicknesses were tested in [9], showing significant mechanical properties reduction. In this case, the
58 corrosion degradation level varied between 17% and 34%. For 25% of degradation level, the observed
59 reduction of yield stress was around 14%. However, in this case, the maximum residual thickness was
60 considered as the reference value for the calculation of mechanical properties.

61 Very thin specimens of 1 mm subjected to atmospheric corrosion were tested in [10], and the observed
62 reduction of mechanical properties reached the level of 70%, for the degradation level of 40%. Also in
63 this case, maximum residual thickness after corrosion was taken as the reference value.
64 Atmospherically corroded specimens with lower values of corrosion degradation were tested in [11],
65 showing that above 15% of degradation level, there is an evident decrease of mechanical properties.
66 Some other works related to the mechanical properties of steel elements subjected to atmospheric
67 corrosion may be found in [12–15].

68 The tensile testing of corroded specimens was also performed regarding circular bars. The stress-strain
69 behaviour of corroded circular bars was investigated by Kashani et al. [16], and the degradation level
70 was up to 20%. The concrete elements with bars were corroded in salt water with the application of
71 electric current. The observed reduction of yield strength was up to 30%, and the total elongation was
72 reduced up to 80%. In the study of Zhan et al. [17], the 267 naturally and artificially corroded specimens
73 have been tested, showing the significant deterioration of mechanical properties and shortening or
74 even disappearing yield plateau. Other works related to the mechanical properties of corroded bars
75 may be found in [18–22], leading to similar conclusions.

76 Based on the listed works, the reduction of mechanical properties of flat-bar specimens as well as bars
77 with the corrosion development was evident. Further, it could be concluded that the reduction of
78 mechanical properties has been observed for both severely degraded specimens and lower corrosion
79 degradation levels related to the steel structures in operation. However, it can be noted that the
80 reduction of mechanical properties is different for different studies. Thus, more experimental work is
81 needed to establish more general relationships accounting for type of corrosion considered. In
82 addition, different reduction levels were obtained for flat-bar specimens and for bars.

83 It was also found, that the reduction of mechanical properties is mainly caused by the local non-
84 uniformities of the surfaces of the corroded specimens [23–26]. For ideally uniformly corroded
85 specimens, the reduction of mechanical properties will be not visible, supported by the experimental
86 results presented in [27]. The specimens after cleaning showed higher mechanical properties than the
87 corroded non-cleaned ones. Additionally, when the FE analysis was performed, taking into account

88 only non-uniformities in corroded surfaces [28,29], the results were similar to those obtained
89 experimentally.

90 In the marine environment and especially for ship structures, general corrosion with local non-
91 uniformities is the most common, and this phenomenon cannot be neglected, and in this respect,
92 mathematical models showing the loss of mechanical properties as a function of corrosion
93 development need to be developed. Some models based on the limited experimental data exist for
94 corroded bars [30–32]. In case of flat-bar specimens, most of studies deals with atmospheric corrosion
95 [9–13]. Only the study performed by Garbatov et al. [7] could be noticed in the case of marine
96 immersed corrosion. However, in this case and most of other studies, the corrosion was accelerated
97 by the application of electric current. It has been shown in [33] that when specimens are corroded with
98 the DC power input source application, the corrosion morphology will be different from those obtained
99 in natural conditions. Higher non-uniformity in thickness distribution is observed for naturally corroded
100 specimens.

101 The presented work extends analyses of the mechanical properties of steel specimens subjected to
102 immersed marine corrosion degradation for a lower corroded level of steel specimens. The previous
103 research was mainly devoted to the specimens subjected to atmospheric corrosion, whereas studies
104 related to marine immersed corrosion are lacking. The limited works related to marine immersed
105 corrosion were focused on rather higher levels of degradation. Furtherly, the corrosion was fastened
106 by the application of electric current. In the present study, the specimens were corroded in laboratory
107 conditions by the acceleration of only natural factors. The detailed information regarding corrosion
108 tests could be found in [34]. Nevertheless, the main features are briefly outlined in the text. Three
109 different groups of thicknesses and different corrosion degradation levels were examined. Based on
110 the tensile test results, the changes in mechanical properties depending on the lower corrosion
111 degradation level were analysed. The bilinear stress-strain model of lower corroded steel plates is
112 proposed for the fitness-for-purpose analyses in the structural integrity assessment.

113 **2 Experimental set-up and corrosion testing**

114 The three different thicknesses of plates made of normal shipbuilding strength steel of S235 (which is
115 also used in other branches of technology under different symbols) were the objective of the current
116 study, namely 5 mm, 6 mm and 8 mm thicknesses. Although corrosion resistant steels are available,
117 due to their high price, the typical constructional steel is commonly used. The chemical composition
118 of steel, as provided by the manufacturer, is presented in Table 1. Although the plates were made from
119 one batch of the steel, the hot-rolling process caused a slight difference in the chemical composition
120 of plates with different thicknesses. Standard coupon specimens (fabricated according to the ISO norm

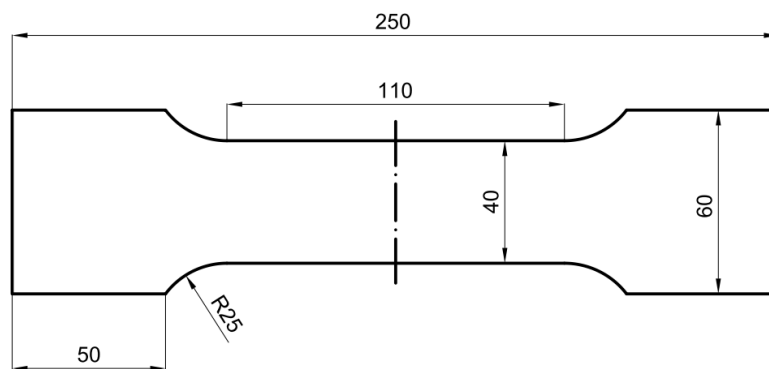


121 [35]) from each thickness of standard size (see Figure 2) were taken from different places of steel
 122 sheets (1.25 m x 2.5 m) and analysed. In each thickness, six or seven specimens were used to obtain
 123 the mechanical properties in an intact state, whereas ten samples were subjected to the accelerated
 124 marine immersed corrosion degradation. In case of intact plates, a such number of specimens provided
 125 a minimum reliable database regarding the mean values of mechanical properties and their scatter. In
 126 case of corroded specimens, such number leads to an examination of changes in mechanical properties
 127 with the corrosion development with the low difference between subsequent degradation levels.

128 Table 1. Chemical composition of tested steel specimens.

Thickness [mm]	Fe [%]	C [%]	Si [%]	Mn [%]	S [%]	P [%]	Cu [%]	Al [%]	N [%]
5	99.2	0.1	0.01	0.48	0.013	0.025	0.04	0.03	0.004
6	99.1	0.12	0.03	0.51	0.011	0.015	0.06	0.03	0.004
8	99.0	0.13	0.024	0.67	0.012	0.023	0.026	0.03	0.004

129



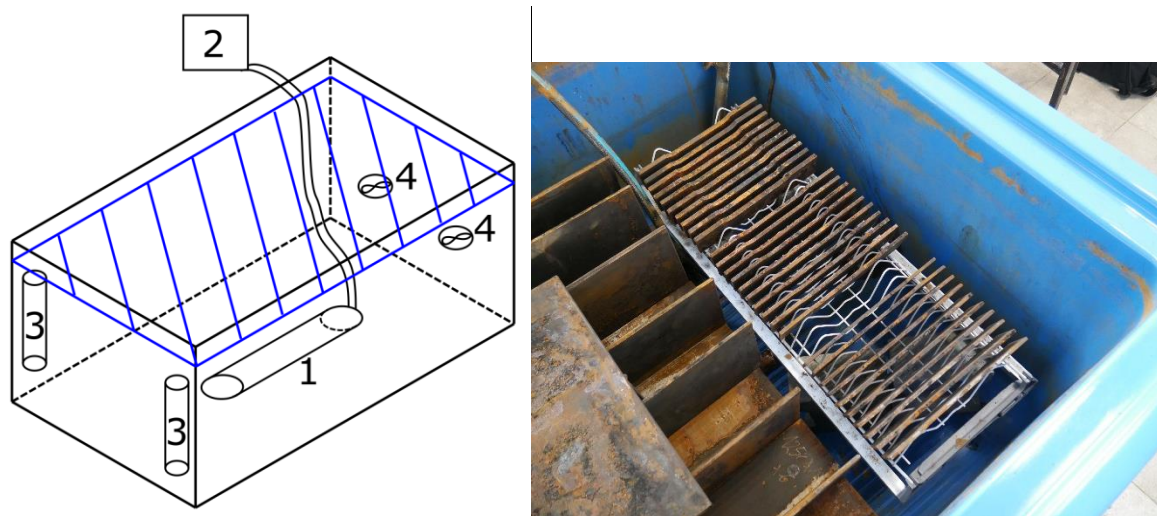
130

131 Figure 2. Dimensions of standard coupon specimens [mm].

132 The corrosion test set-up has been already presented in [36], and the results of corrosion tests have
 133 been widely discussed in [34]. Thus, only main information regarding corrosion testing is provided.

134 The coupon specimens were corroded in a 900-litre tank made from glass reinforced plastic laminate,
 135 together with larger-sized stiffened plates. The corrosion testing set-up is presented in Figure 3,
 136 showing the small-scale specimens placed on the supporting structure. The corrosion rate was
 137 increased by the aeration pump (2) (oxygen content increase), heaters (3) (temperature increase) and
 138 circulation pumps (4). The salinity level was set equal to 35 ppm by mixing freshwater with natural sea
 139 salt. The governing parameters were initially assumed: 35°C, 300% oxygen content concerning
 140 supersaturation conditions, and a water speed of 0.03 m/s. The corrosion rate estimated initially was

141 equal to 0.736 mm/year [36]. The corrosion testing tends to provide a specific level of degradation
142 within initially assumed time frames, where the governing factors were constant. Corrosion testing
143 could also possibly account for natural temperature or water velocity fluctuations. This could be done
144 by setting the temperature controller and circulation pumps controller for specific function that will
145 change the factors within time. However, in present study, factors were assumed to be constant. The
146 total duration of the corrosion test was 428 days. Additional circulation pumps have been applied to
147 increase the water velocity due to the lower oxygen level than initially assumed (around 200%). The
148 mean corrosion rates were 0.649 mm/year, 1.009 mm/year and 1.025 mm/year for 5 mm, 6 mm and
149 8 mm specimens, respectively [34].



150

151 Figure 3. Corrosion test set-up [34] (1- linear diffuser, 2 – aeration pump, 3 - heaters, 4 – circulation
152 pumps) (left) and corrosion tank with placed specimens (right).

153 The target levels of corrosion degradation, that were aimed to achieve during the design of set-up
154 were: 3%, 6%, 8%, 10%, 12%, 14%, 16%, 18%, 20%, 21%, which respect the operational level of
155 corroded steel plates before they are replaced at 25% degradation in structures in operation. Due to
156 an increasing level of uncertainty in the severe corrosion degradation, the intervals of the degradation
157 level were smaller for severely corroded specimens. The final corrosion degradation levels, obtained
158 from mass measurements, are presented in Table 2. Additionally, the corrosion surface's statistical
159 descriptors are obtained based on the information gathered from the scanning of the specimens, as
160 described in [34], including maximum and minimum thickness, minimum cross-sectional area and
161 standard deviations of corrosion diminutions. Notably, a significant level of surface non-uniformity was
162 observed (see Figure 4, bottom).

163 Both surfaces of the specimens were scanned separately. In some cases, the standard deviation of the
164 corrosion depth measured in one side of the specimen reached the level of 0.84 mm. Before

165 measurements, the specimens were cleaned. The scanning provided information about the surface
166 non-uniformities (only one surface could be scanned at a time), whereas degradation level was
167 obtained based on mass measurements. The example of the corroded specimen after cleaning, during
168 scanning, is presented in Figure 4.



169



170

171 Figure 4. Example of the specimen during scanning (top) and example of reproduced surface
172 (bottom).

173 It needs to be highlighted that actual degradation levels were slightly different from those assumed
174 initially. There were two reasons for that. Firstly, the specimens were cleaned after corrosion
175 degradation. The actual mass was somewhat lower than that measured directly after testing. Secondly,
176 for strength evaluation, only corrosion characteristics of specimens without mounting parts are
177 relevant. Thus, based on the scanning results, the degradation level of the gauge part was determined.

178 In most cases, the differences were not exceeding 2 % of degree-of-degradation (*DoD*), concerning
179 the degradation level for the whole specimen. The *DoD* level is considered as the percentage of the
180 initial mass of the specimen due to corrosion degradation. Thus, it is the mean level of corrosion
181 degradation of each specimen. The *DoD* will depend on the time of corrosion degradation, which could

182 be noticed in [34]. However, for strength testing, the *DoD* level is the most important. The final
 183 degradation levels for each thickness are presented in Table 2. The mechanical properties were
 184 determined according to mean thickness after corrosion degradation, i.e. accounting for degradation
 185 levels shown in Table 2. Determining mechanical properties concerning the mean value of thickness is
 186 practical since it can be obtained by ultrasonic measurements periodically performed in ships and
 187 offshore structures. Based on the mean thickness reduction, the *DoD* and changes in mechanical
 188 properties may be estimated. Further, as *DoD* increase, the level of surface non-uniformity also
 189 increase. Thus, *DoD* accounts for non-uniformity in corroded surfaces implicitly, but is more practical
 190 to be determined in operating structure.

191 Table 2. Degradation levels of specimens, considering gauge section only.

Thickness [mm]	Degradation level in ascending order for subsequent specimens [%]									
	No. 1	No. 2	No. 3	No. 4	No. 5	No. 6	No. 7	No. 8	No. 9	No. 10
5	3.2	5.9	7.4	8.0	13.1	15.4	15.4	15.5	16	24.3
6	2.2	6.3	6.8	9.6	12.3	14.1	14.7	16.6	17.6	21.3
8	1.7	4	12.3	13.8	14.1	14.8	15.6	16.9	18.4	28.4

192

193 The standard Zwick-Roell Z400 machine with a step electric engine was used to conduct the tensile
 194 test and estimate the elasticity modulus, where a mechanical extensometer was adopted (see Figure
 195 5). The tests were performed following the ISO standard for tensile testing [35] of flat coupons, and
 196 the loading was displacement-driven. The strain rate was 0.00025 mm/mm/s up to the moment, where
 197 the yield point has been reached. Above the yield point, the strain rate was 0.002 mm/mm/s. The
 198 distance between heads was 170 mm.



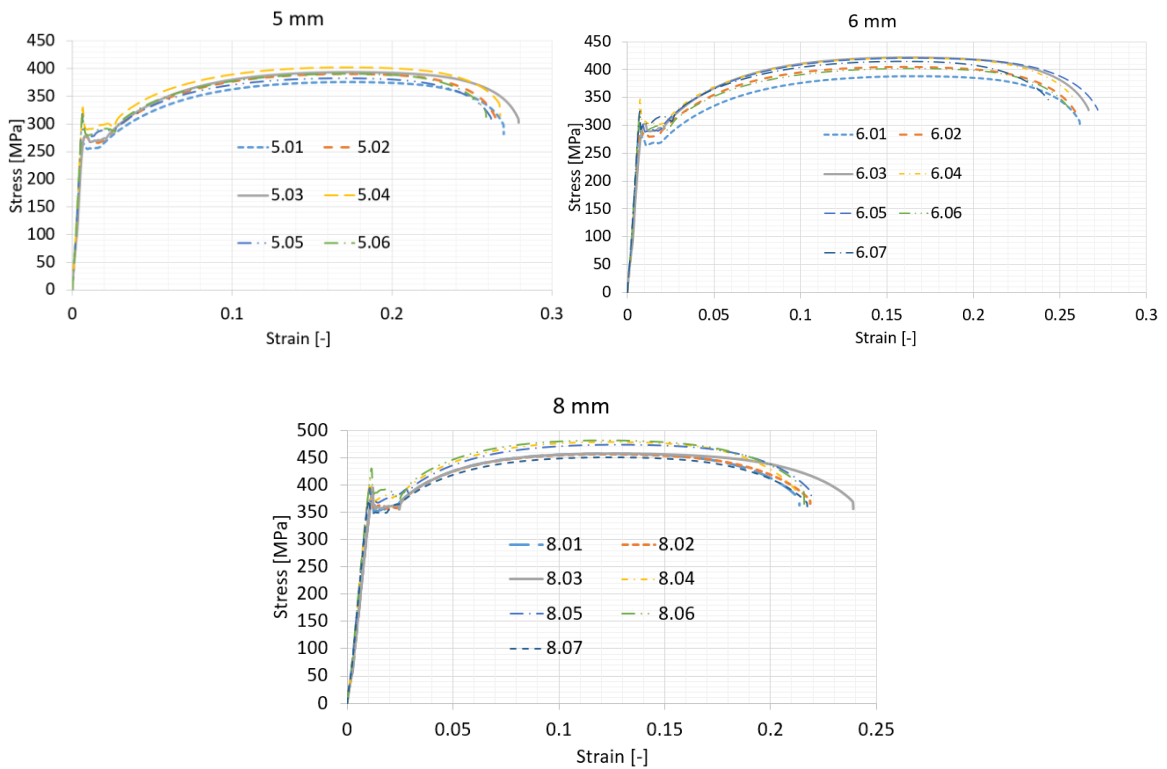


199

200 Figure 5. Testing machine (left) and mounted specimen with installed extensometer (right).

201 **3 Stress-strain behaviour of intact specimens**

202 Six to seven intact specimens of each thickness were tested before corrosion degradation to identify
 203 the initial mechanical properties. The obtained engineering stress-strain curves are presented in Figure
 204 6.



205

206

207

Figure 6. Stress-strain curves for 5 mm, 6 mm and 8 mm intact specimens.

208 The summary of performed tensile tests is presented in Table 3. In the case of elastic modulus, very
 209 similar results in different thicknesses were obtained. However, for both yield stress and ultimate
 210 tensile stress, the values are different for each thickness. The yield stress has been considered the
 211 lower yield point. The elastic modulus was calculated as the mean inclination of the stress-strain curve
 212 in the region between 20 % and 80 % of the yield stress. Notably, the yield stress value is higher than
 213 the normative value of 235 MPa for that steel grade. The 5 mm and 6 mm specimens presented similar
 214 total elongation, whereas 8 mm specimens were of the lower ductility. It could also be noted that some
 215 features typical for the material type rather than thickness are similar, i.e. evident yield plateau and
 216 stress-strain relationship after the beginning of yielding. Further, the mechanical properties are
 217 subjected to a significant level of uncertainty. The highest uncertainty is observed for a 5 mm plate in
 218 the yield stress, and the Coefficient of Variation is 4.5 %. In general, the level of uncertainty oscillates
 219 between 3 % and 4.5 % of CoV for different properties.

220

221 Table 3. Tensile tests for intact specimens.

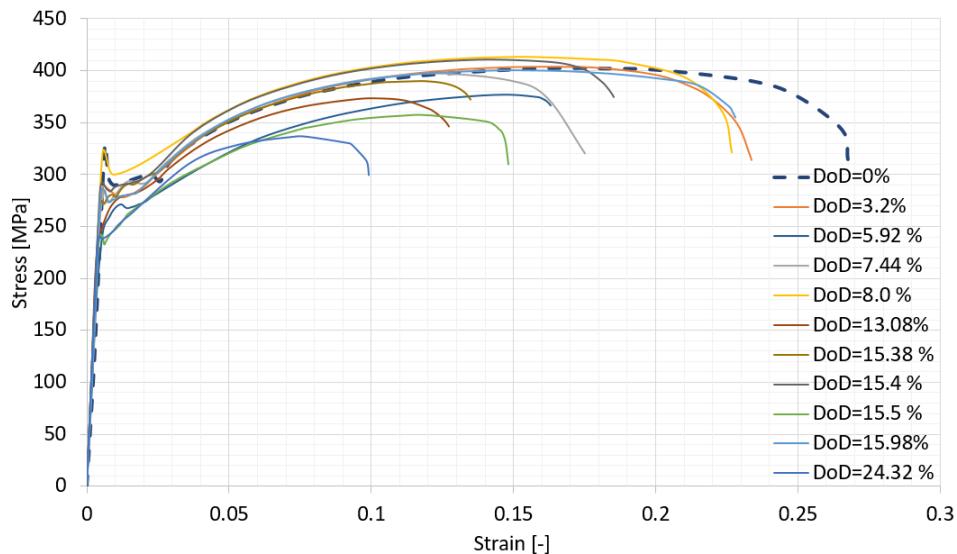
Thickness [mm]	Parameter	Young's modulus E [GPa]	Yield stress R_e [MPa]	Ultimate tensile stress R_m [MPa]	Total elongation δ [-]
5	Mean	197.42	272.25	389.19	0.266
	Standard Deviation	10.43	12.31	9.15	0.01
	Coefficient of Variation [-]	0.053	0.045	0.024	0.027
6	Mean	196.38	284.36	410.30	0.260
	Standard Deviation	7.57	12.57	12.66	0.01
	Coefficient of Variation [-]	0.039	0.044	0.031	0.034
8	Mean	199.08	360.61	465.15	0.219
	Standard Deviation	6.84	11.83	12.55	0.01
	Coefficient of Variation [-]	0.034	0.033	0.027	0.041

222

223 4 Stress-strain behaviour of corroded specimens

224 After cleaning and measuring the corroded specimens, there were subjected to tensile testing. As a
 225 result, the stress-strain relationship for each specimen has been obtained, and all testing parameters
 226 have been registered. The stresses were calculated regarding the mean thickness value, estimated
 227 based on the degradation level, as reported in Table 2.

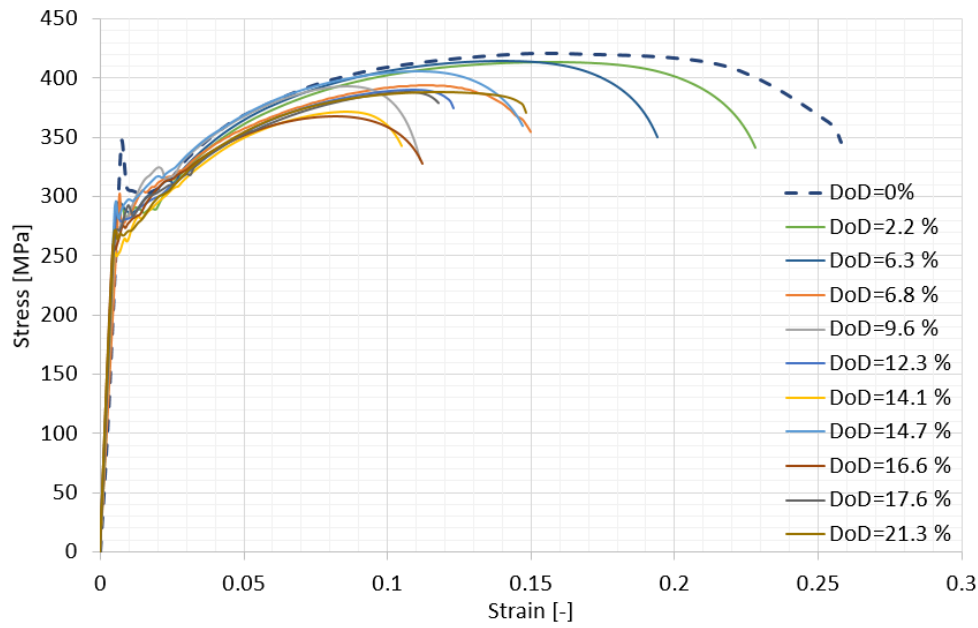
228 The stress-strain relationships for 5 mm specimens for different *DoD* were presented in Figure 7.
229 Additionally, the reference stress-strain curve, for *DoD* = 0% was added, which was taken from tests
230 of intact specimens. The curve that resulted in the highest value of yield stress from several specimens
231 was considered in this case. This graph shows evident degradation of mechanical properties, including
232 the yield stress, ultimate tensile stress, and total elongation. Further, the yield plateau is smaller with
233 corrosion development and even disappearing for severely corroded specimens than intact specimens
234 (see Figure 6).



235

236 Figure 7. Stress-strain relationships for 5 mm specimens subjected to corrosion degradation

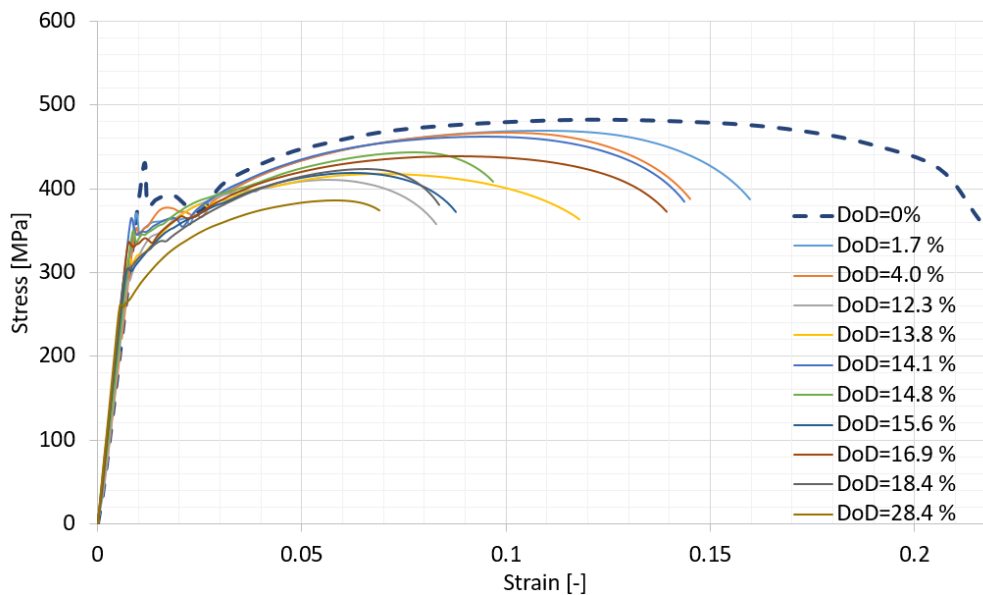
237 Similar observations could be captured for other groups of thicknesses. The stress-strain relationships
238 for 6 mm specimens are presented in Figure 8, whereas for the 8 mm specimens are shown in Figure
239 9. The most evident differences in changes in the yield stress could be noticed in Figure 9 for the 8 mm
240 specimens. In the 6 mm specimens, those changes are smaller (see also Table 4). Nevertheless, a lack
241 of the yield plateau for severely corroded specimens and a significant drop of total elongation is purely
242 visible in both cases.



243

244

Figure 8. Stress-strain relationships for 6 mm specimens subjected to corrosion degradation



245

246

Figure 9. Stress-strain relationships for 8 mm specimens subjected to corrosion degradation

247

248

249

250

251

252

253

254

The detailed results are presented in Table 4. From the beginning, a large scatter of mechanical properties is observed. There are two sources of this phenomenon. Firstly, significant scatter was observed for the intact specimens of mechanical properties (see Table 3). Secondly, since the corrosion process introduces a stochastic origin, the mechanical properties are dependent on those, resulting in additional scatter. Thus, to observe the relation between *DoD* and mechanical properties, there were grouped by similar degradation levels, i.e., group 1 (between 0 % and 8 % of *DoD*), group 2 (between 8 % and 16 % of *DoD*) and group 3 (above 16 % of *DoD*). Additionally, one point from 5 mm thickness was excluded from further analysis due to the very high yield stress and ultimate tensile stress values,

255 exceeding the maximum values observed for intact specimens (see Figure 7). The division of specimens
 256 into groups is presented in Table 4 regarding each thickness.

257

258

259

260

261

262

263

264

265 Table 4. Detailed results of mechanical properties for corroded specimens.

Thickness [mm]	DoD [%]	E [Gpa]	R _e [Mpa]	R _m [Mpa]	Elongation [-]	Group
5	3.2	234.8	278.1	404.0	0.234	1
	5.9	208.0	253.2	377.0	0.163	
	7.4	219.9	273.1	397.5	0.175	
	8.0	202.1	300.0	413.3	0.227	excluded
	13.1	238.0	247.9	373.6	0.127	2
	15.4	236.9	271.7	389.8	0.134	
	15.4	256.6	283.6	410.3	0.185	
	15.5	221.1	232.7	356.9	0.148	
	16.0	235.5	273.8	400.0	0.228	3
	24.3	187.1	238.0	336.6	0.099	
6	2.2	192.9	281.3	413.5	0.229	1
	6.3	200.8	286.1	414.5	0.195	
	6.8	203.0	273.5	393.4	0.150	
	9.6	211.9	270.0	392.8	0.112	2
	12.3	242.1	278.3	390.1	0.123	
	14.1	202.4	249.7	371.5	0.106	
	14.7	247.4	281.0	405.3	0.151	
	16.6	214.7	255.1	367.9	0.113	
					3	

	17.6	258.6	271.3	387.7	0.119	
	21.3	208.5	264.3	388.6	0.148	
	1.7	221	343.8	469.5	0.161	1
	4.0	234.1	344.5	467	0.146	
	12.3	226.3	307	410.8	0.083	
	13.8	215.6	310.2	417.2	0.118	
	14.1	220.6	344.8	462.1	0.144	2
8	14.8	226.1	335.3	443.1	0.098	
	15.6	187.5	299.9	418.6	0.088	
	16.9	219	334.5	438.4	0.14	
	18.4	222.7	303.2	423.2	0.084	3
	28.4	204.5	258.4	385.8	0.069	

266

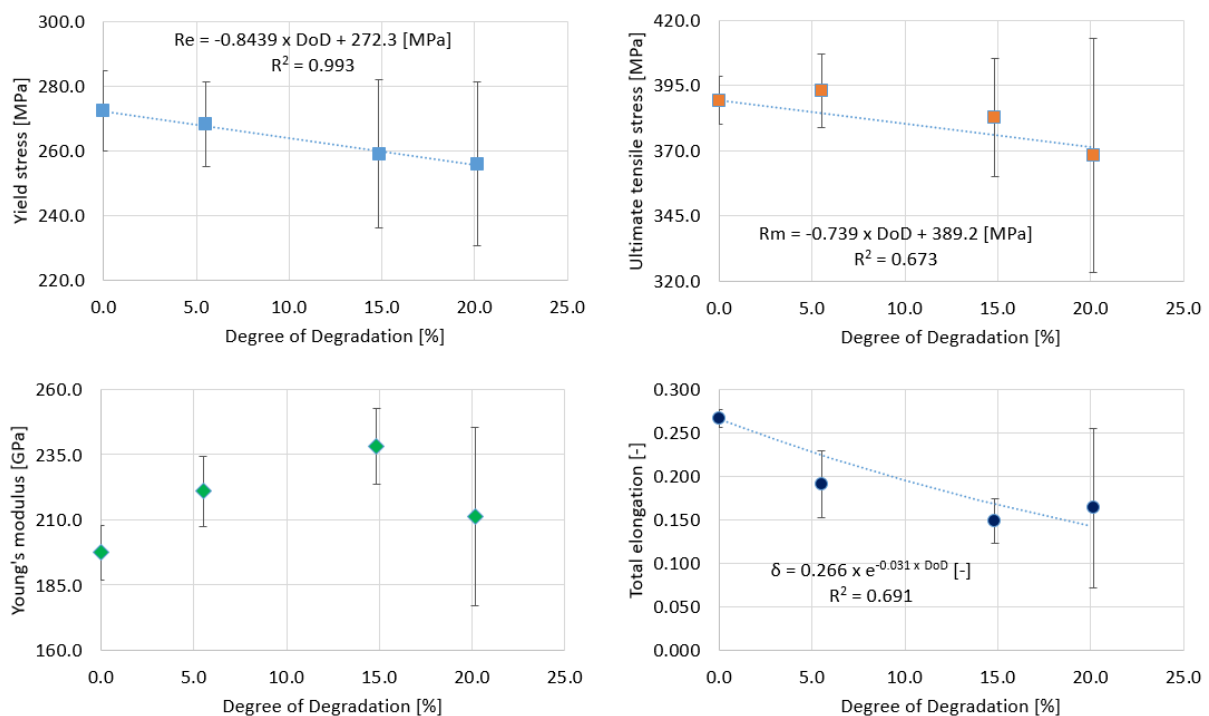
267 To investigate the changes in mechanical properties with the progress of corrosion degradation, the
 268 results for each thickness are plotted as a function of the Degree of Degradation. For each group, the
 269 mean value of both *DoD* and respective mechanical properties is calculated. Thus, the points in graphs
 270 are not representing the values for particular specimens but mean values for different groups of
 271 degradation levels (groups 1, 2 and 3), as presented in Table 4. Additionally, the error bars showing
 272 the standard deviation of each group are presented. The corrosion dependent mechanical properties
 273 for 5 mm specimens were presented in Figure 10. The mechanical properties for *DoD* = 0 % are
 274 considered as the mean value from tensile tests performed for intact specimens and there are reported
 275 in Table 3 for each thickness separately.

276 Further, the regressions are found, considering that for *DoD* = 0%, the values are known and equal
 277 to initial values. As outlined in the last part of the text, the results of Young's modulus were inaccurate
 278 and thus, no regressions were established. This methodology is adopted similarly for other thicknesses.

279 The evident reduction of mechanical properties is observed. In the case of yield stress and ultimate
 280 tensile stress, the linear regressions are plotted. There were found to have the highest correlation for
 281 different thicknesses. For total elongation, the exponential regression was found to represent its
 282 changes with corrosion development. Although a similar correlation factor is found for the linear
 283 regression, this will result in negative values of that parameter for higher values of *DoD*. In the case of
 284 exponential regression, the value will always be positive and tend to be near-zero value for *DoD* =
 285 100 %. The observed correlation factors for the yield stress is very high, whereas lower values were
 286 obtained for ultimate tensile stress and total elongation.

287 However, there was found no correlation between Young's modulus and degradation level. Very high
 288 elastic modulus values were obtained for some mean corrosion depths, significantly exceeding its
 289 value for intact specimens, even considering uncertainty level (see Figure 10). Thus, such values
 290 obtained experimentally should be considered false. The same observation is obtained for other
 291 thicknesses, i.e. 6 mm (Figure 11) and 8 mm (Figure 12).

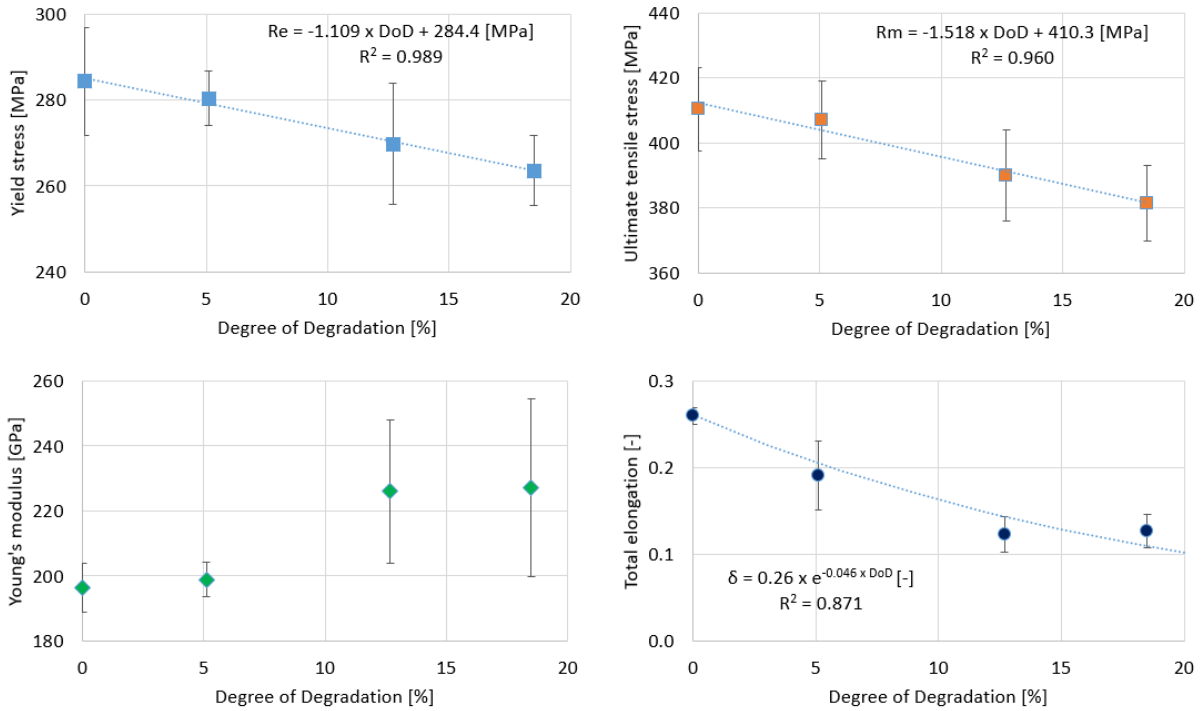
292 There are several possible reasons for such a situation. In the case of the yield stress, ultimate stress
 293 and total elongation, these characteristics somehow represent the entire specimen's behaviour.
 294 However, in Young's modulus, the strain is measured via an extensometer between two points near
 295 the specimen's middle. In the prismatic specimen, this is purely valid, whereas, in the case of a
 296 corroded specimen, this does not show the entire specimen's behaviour. As reported by corrosion
 297 scans, there are cases with areas of a higher thickness in the middle of the specimen, which will lead
 298 to relatively low strains when the mean thickness is considered a reference. Notably, the places of
 299 failure of the specimens were, in most cases, away from the middle (see Figure 13). Thus, the obtained
 300 Young's modulus for the corroded specimens cannot be considered. The elastic modulus could be
 301 considered a constant for the whole *DoD* range and equal to the one obtained for intact specimens.



302

303 Figure 10. Mechanical properties as a function of DoD, 5 mm specimens.

304 The changes in mechanical properties for 6 mm specimens are presented in Figure 11. It is noted that
 305 there was observed a similar reduction of the yield stress, whereas ultimate tensile stress degraded
 306 faster in comparison to 5 mm specimens. It is noted that very high correlation factors were obtained
 307 for each mechanical property (except for elastic modulus).



308

309

Figure 11. Mechanical properties as a function of DoD, 6 mm specimens.

310

The corrosion-dependent mechanical properties for the 8 mm specimens are presented in Figure 12.

311

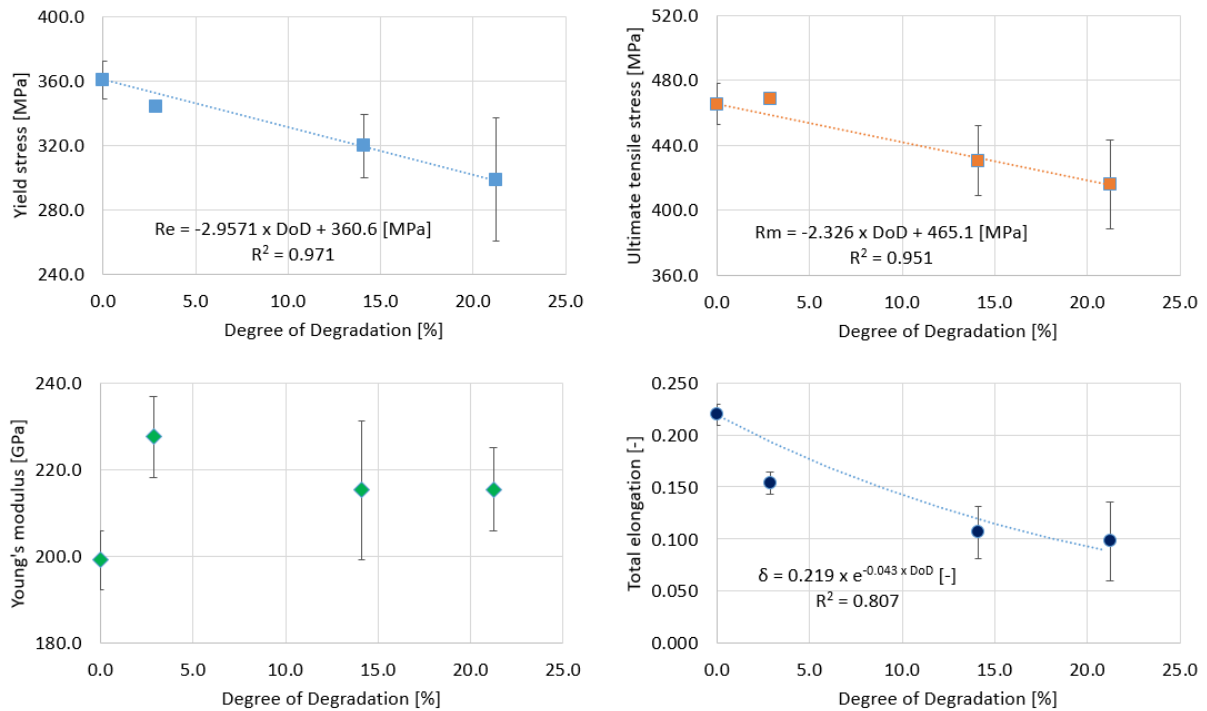
Notably, the observed reduction of mechanical properties is significantly higher than other

312

thicknesses, regardless of the higher initial values of the yield stress and ultimate tensile stress (see

313

Table 3). Similarly to 6 mm specimens, very high correlation factors has been observed.



314

315

Figure 12. Mechanical properties as a function of DoD, 8 mm specimens.

316 It could also be noted that lower correlation coefficient values have been observed in the case of 5
317 mm plates (Figure 10). It could be concluded that the lower correlation for 5 mm plates was caused by
318 relatively high uncertainty of both material properties and corrosion characteristics. Notably, for 8 mm
319 plates, a higher decrease of material properties has been observed, which dominated the observed
320 scatter of the results.

321 By comparing the presented results with other available data, it is noted, that with comparison to
322 marine immersed corrosion accelerated with the application of electric current [7], higher reduction
323 of yield stress was observed. In the case of the present study, for $DoD = 25\%$, the yield stress was
324 reduced by approximately 10%. In the case of [7], a 15% reduction was noted for $DoD = 50\%$. When
325 compared with naturally atmospherically corroded specimens [9], the observed reduction for $DoD =$
326 25% was similar to the present study. However, the maximum residual thickness was considered as
327 the reference to calculate the mechanical properties.

328 Figure 13 shows examples of failure modes of tested specimens. It could be noticed that the failure
329 mode is different in comparison to typically observed for intact specimens. In most cases, the cross-
330 section, where the breaking line is followed, is related to the position, where the minimum cross-
331 sectional area along the gauging part is located [29]. Further, the breaking line is non-straight and
332 inclined in most cases, which is not the case of intact specimens, where a straight line is usually noted
333 perpendicular to the loading direction.



334

335

336

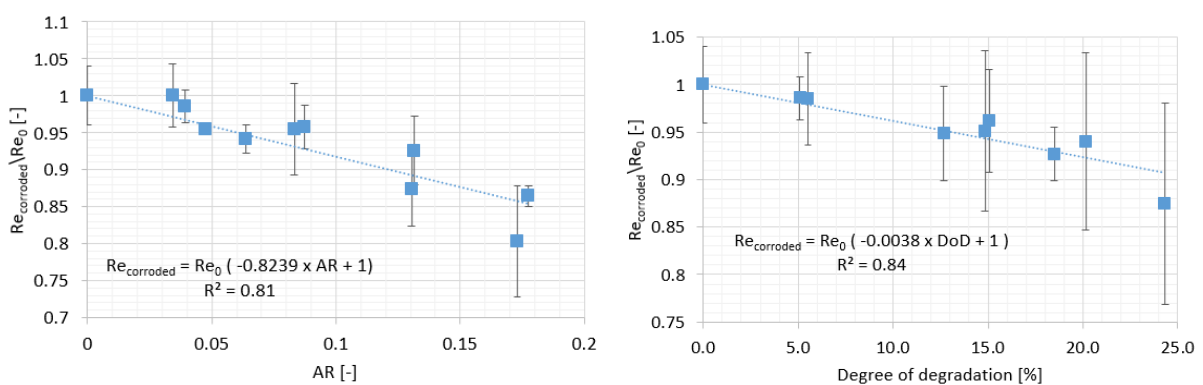
337 Figure 13. The examples of tested specimens with a thickness of 5 mm (top), 6 mm (mid) and 8 mm
338 (bot).

339 Different studies noted that the yield stress's degradation level is most probably related to the
 340 minimum cross-sectional area obtained along with the specimen. Therefore, to verify that, the
 341 normalised yield stress (yield stress of corroded specimen divided by the mean yield stress of intact
 342 specimen) is compared with the normalised reduction factor of minimal cross-sectional area. In this
 343 case, the results for single specimens are investigated since the area reduction is related to any
 344 particular specimen. However, since the material properties are estimated based on the cross-
 345 sectional area, which is associated with the mean value thickness of the corroded specimen, the
 346 normalised reduction factor of cross-sectional area is proposed as follows:

$$347 \quad AR = \frac{A_0 \left(1 - \frac{DoD}{100}\right) - A_{min}}{A_0 \left(1 - \frac{DoD}{100}\right)} [-] \quad (1)$$

348 where A_0 is the initial cross-section area of non-corroded specimen and A_{min} is the minimum cross-
 349 sectional area.

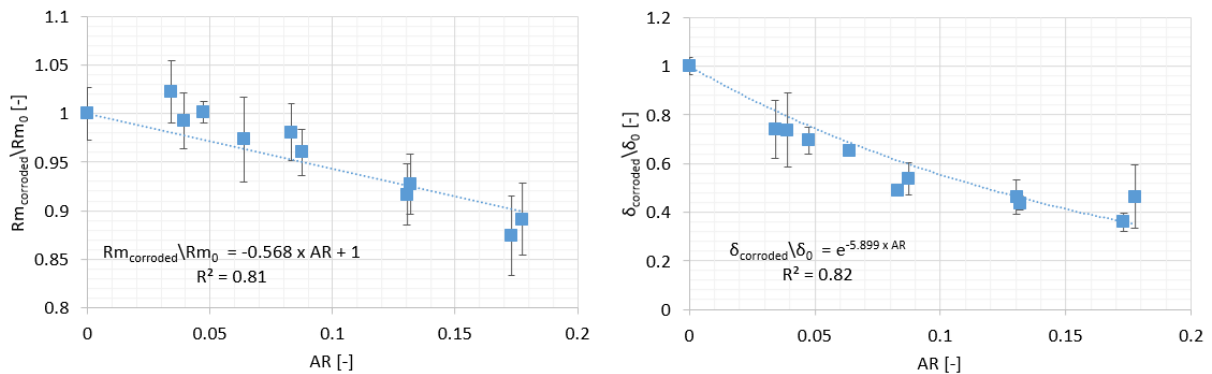
350 The proposed factor informs how much the minimum cross-sectional area is smaller concerning the
 351 mean cross-sectional area. In other words, factor shows the percentage difference between minimum
 352 cross-sectional area and cross-sectional area, if corrosion will cause the uniform reduction of thickness.
 353 The bigger the AR factor is, the smaller the cross-sectional area is as a percentage of the mean cross-
 354 sectional area of the corroded specimen. Figure 14 (left) shows the results from different thicknesses
 355 collated and the relation between the yield stress and reduction factor. A similar statistical analysis, as
 356 in the case of Figures 10 to 12 was adopted herein. Thus, the experimental points were grouped within
 357 similar AR factors levels, and each group's standard deviation is presented in the graph.



358
 359 Figure 14. Relation between normalised yield stress and cross-sectional area reduction factor (left)
 360 and between normalised yield stress and DoD (right).

361 It is noted that a good correlation between these two parameters is observed. Except for several
 362 points, the observed scatter is in the order of yield stress uncertainty. Although a similar correlation
 363 between the reduction factor and yield stress was achieved compared to DoD and yield stress (see

364 Figure 14 - right), the scatter for particular groups is significantly smaller. The linear correlation was
 365 the most suitable for both cases presented in Figure 14, resulting in the highest correlation coefficient.
 366 This indicates that not always the degradation level is the most appropriate parameter that informs
 367 about the state of a corroded structure. A similar correlation was found between area reduction factor
 368 and normalised ultimate tensile strength and normalised total elongation, respectively (see Figure 15).
 369 In the case of ultimate tensile strength, the linear correlation resulted in the highest correlation factor,
 370 whereas, the exponential regression was most appropriate for a total elongation. Similarly to the yield
 371 stress, the area reduction factor is more related to the corrosion-dependent material properties than
 372 the Degree of Degradation level. The correlations between *DoD* and normalised ultimate tensile stress
 373 and total elongation were 0.59 and 0.71, respectively (see Figure 16). Similarly to yield stress, the single
 374 data points are significantly less scattered with comparison to the regressions based on *DoD* (see
 375 Figure 16).



376

377 Figure 15. Relation between cross-sectional area reduction factor and normalised ultimate tensile
 378 strength (left) and normalised total elongation (right).

379 Although *AR* factor seems to be more suitable to predict the degradation of material properties, its
 380 determination requires very detailed surface recognition. Thus, for engineering applications, *DoD* is
 381 more convenient, estimated based on simple thickness measurements. Additionally, by grouping the
 382 results, the compensation of uncertainty related to area reduction may be obtained.

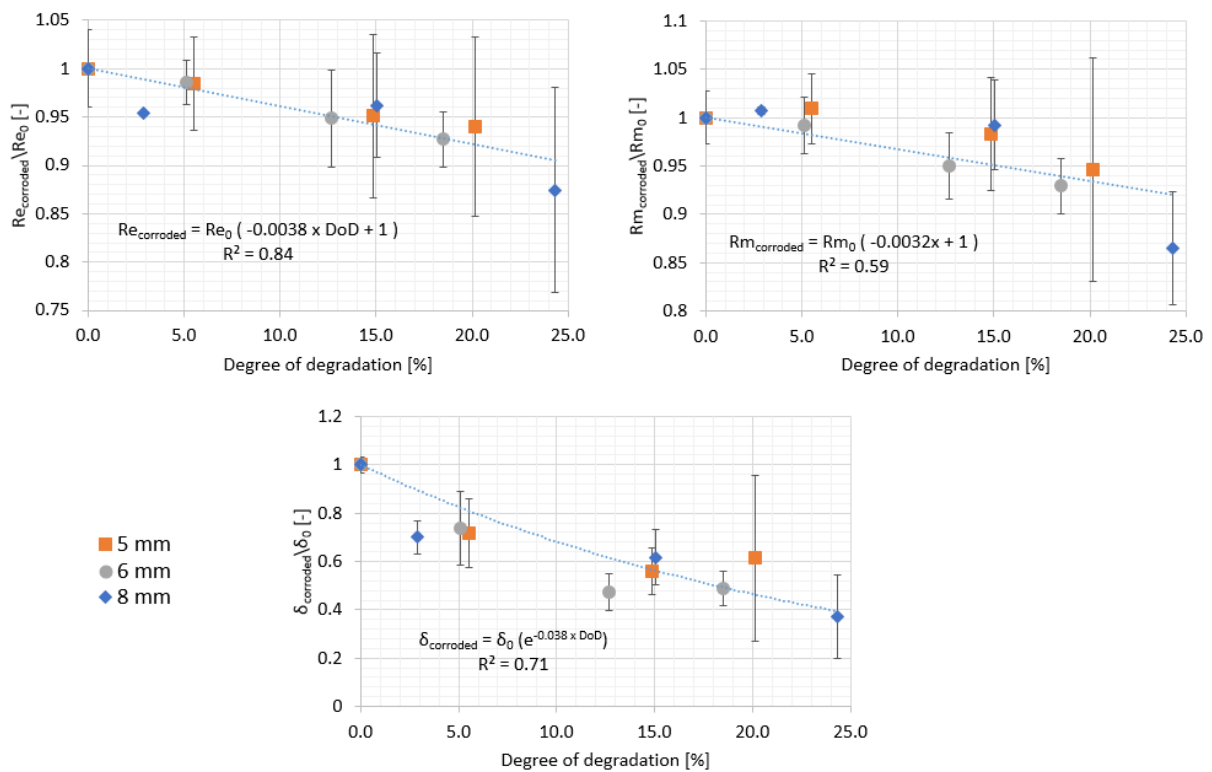
383 Based on the presented results, one could draw the hypothesis that the thicker plate is, the higher
 384 reduction of mechanical properties is observed. However, it will be somewhat premature to make
 385 conclusions, and more investigations will be needed at this stage. Especially, there were no significant
 386 differences in reduction levels in the case of 5 mm and 6 mm specimens, and only 8 mm specimens
 387 presented a higher level of mechanical properties decrease. It could result from slightly different
 388 corrosion characteristics obtained for a diverse group of thicknesses. It was found that the area
 389 reduction factor was the main reason for the deterioration of material properties. This factor was
 390 slightly higher for the 8 mm specimens than others, and thus, the material properties were also lower.

391 **5 Stress-strain model for fitness-for-purpose analyses**

392 Since the mechanical properties themselves are subjected to relatively high scatter, it is reasonable to
393 consider changes in mechanical properties obtained from various initial thicknesses. This will increase
394 the total number of experimental points and derive some constitutive laws regardless of the
395 specimen's initial thickness, which could be helpful to fitness-for-purpose analyses.

396 Since different initial mechanical properties were obtained for different thicknesses, the relative values
397 of mechanical properties with the corrosion degradation progress are estimated. Thus, for a particular
398 DoD, the observed value of the parameter is divided by its value in a non-corroded state. Young's
399 modulus is assumed to be constant within the whole *DoD* range.

400 Figure 16 presents the collected results obtained from the tested specimens (considering results for
401 groups), and the regression relationships have been derived, leading to general constitutive laws.
402 Similarly to previous relationships (Figures 10-12), the linear regression led to the highest regression
403 coefficients for yield and ultimate tensile stresses. In the case of total elongation, both linear regression
404 and exponential one resulted in a similar regression coefficient. However, the exponential was chosen
405 to avoid negative values of the total elongation for higher values of the degradation level, similarly as
406 in Figures 10-12.



407
408 Figure 16. Normalised mechanical properties in function of *DoD*.

409 The standard deviation is calculated since any particular point is scattered from the assumed
 410 regression relationship. The variation for a specific point is calculated as a difference between the
 411 experimental and predicted values by the regression model. In Young's modulus, the standard
 412 deviation is calculated based on the tests carried out for the intact specimens (see Table 3).

413 The standard deviation results are as follows (Young's modulus – Eq. 2, Yield stress – Eq. 3, Ultimate
 414 tensile stress – Eq. 4, Total elongation – Eq. 5):

$$415 \quad E_{StDev} = 0.0402 E_0 [GPa] \quad (2)$$

$$416 \quad Re_{StDev} = 0.0556 Re_0 [MPa] \quad (3)$$

$$417 \quad Rm_{StDev} = 0.0431 Rm_0 [MPa] \quad (4)$$

$$418 \quad \delta_{StDev} = 0.145 \delta_0 [-] \quad (5)$$

419 The presented parameters could be used for the reliability analysis of ship structural components
 420 subjected to corrosion degradation, e.g. [37,38].

421 Further, for a different type of FE analysis, usually, the bilinear stress-strain model is used. It needs to
 422 be noted that a true stress-strain relationship should be used instead of an engineering one. According
 423 to [39], the true stress-strain relationship from the start of yielding up to the moment where the
 424 maximum load is reached could be determined via the following equation:

$$425 \quad \sigma = K \varepsilon^n \quad (6)$$

426 where n is the strain hardening exponent, K is the strength coefficient and ε_p is the plastic strain.

427 To identify the parameters K and n , the log-log plot of the relationship from Eq. 6 could be established,
 428 leading to the linear relationship and fitted to the experimental data from all specimens. The stress-
 429 strain relationship in the logarithmic scale will be the linear relationship followed by the equation $y =$
 430 $ax + b$, where a is equal to n and b is the logarithm of K .

431 Further, to identify the failure strain in a bilinear model, the modulus of toughness could be useful,
 432 given by the equation:

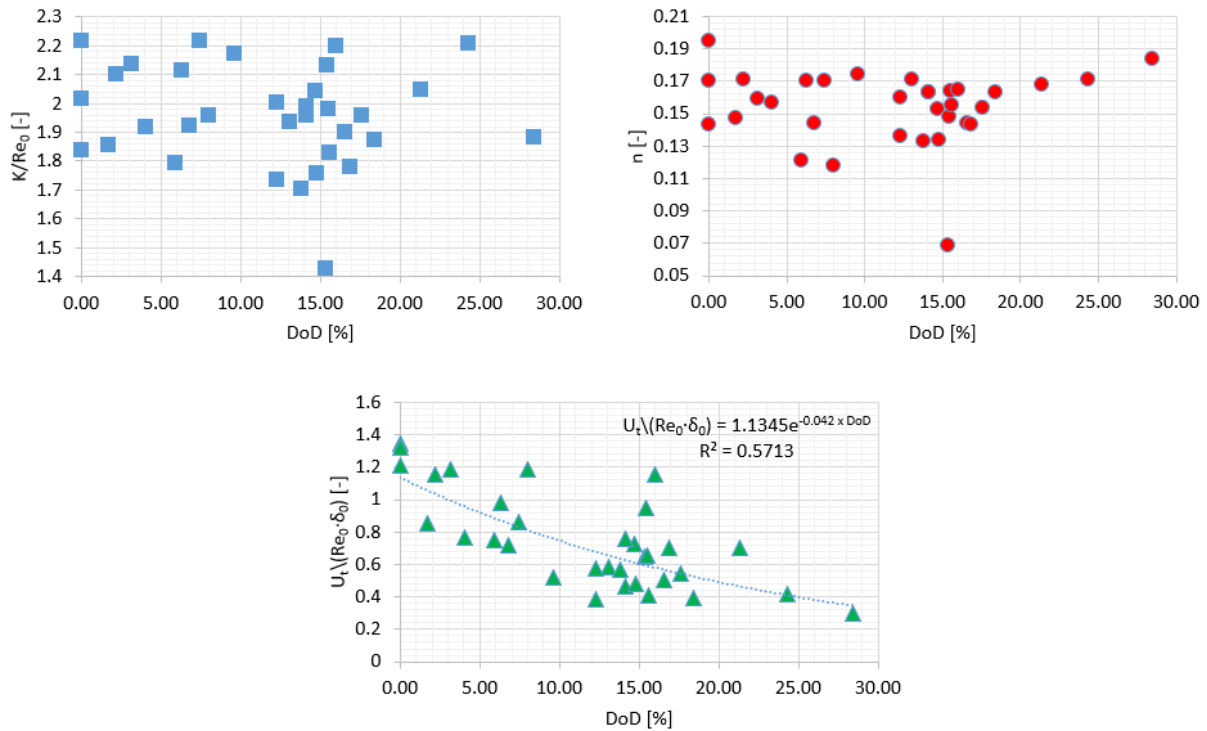
$$433 \quad U_t = \int_0^{\varepsilon_f} \sigma d\varepsilon \quad (7)$$

434 which represents the energy that is needed to break the specimen.

435 The values of K , n and U_t were identified for each specimen. However, since different initial material
 436 properties were observed for different thicknesses, the normalised parameters were introduced,



437 except the strain hardening parameter. The strength coefficient is divided by the initial yield stress of
 438 considered thickness, and the modulus of toughness is divided by the multiplication of yield stress and
 439 total elongation value. The relationships between degradation level and normalised parameters are
 440 presented in Figure 17.



441
 442 Figure 17. Relationships between normalised parameters of stress-strain relationships and
 443 degradation level.

444 The regression analysis was performed and different functions were studied for all variables. For the
 445 normalised strength the R^2 value is not exceeding 0.02, and in the case of the strain hardening
 446 parameter, the regression coefficient was 0.2 for the polynomial regression. It could be concluded that
 447 there is no correlation between these variables and DoD . Thus, the mean values of $K/Re_0 = 1.958$
 448 and $n = 0.154$ are considered. In the case of modulus of toughness, the non-linear regressions were
 449 found to result in highest R^2 values – namely, the polynomial and exponential ones. However, the
 450 polynomial function presented a local minimum for DoD equal to 30%, and the modulus of toughness
 451 will increase after crossing that value. This will be non-concise with the physical representation of the
 452 phenomena. Thus, the exponential equation has been found for the normalised modulus of toughness,
 453 as given in Figure 17.

454 Based on the information provided in both Figures 16 and 17, the bilinear stress-strain relationships
 455 dependent on corrosion level are defined as follows (considering DoD up to 25 %):

$$\begin{aligned}
& E\varepsilon && (\varepsilon < \varepsilon_1) \\
& \sigma_1 = Re_0(1 - 0.0061 \cdot DoD) && \left(\varepsilon = \varepsilon_1 = \frac{\sigma_1}{E}\right) \\
456 \quad \sigma = & \sigma_1 + \frac{(\varepsilon - \varepsilon_1)(\sigma_2 - \sigma_1)}{\varepsilon_2 - \varepsilon_1} && (\varepsilon_1 < \varepsilon < \varepsilon_2) \\
& \left\{ \begin{aligned} & \sigma_2 = \sigma_1 + 1.958 \cdot Re_0 \cdot \varepsilon_2^{0.154} && (\varepsilon = \varepsilon_2) \end{aligned} \right. && (8)
\end{aligned}$$

457 where ε_2 is defined in that the area under the bilinear stress-strain relationship is equal to the modulus
458 of toughness for the particular degradation level.

459 **Conclusions**

460 The presented study investigated the mechanical properties of corroded steel subjected to immersed
461 marine corrosion degradation. It was found that even for a lower degradation level (below 25%), with
462 comparison to previously conducted studies (e.g. [7]), the mechanical properties of mild steel could
463 have significantly deteriorated. This is highly important since such levels of degradation are typically
464 allowed in the operating ship and offshore structures. By comparing the presented results with other
465 available data, it was found that marine immersed corrosion brings the higher decrease of mechanical
466 properties. Notably, not only strength characteristics were deteriorated, but deformability (i.e. total
467 elongation) was significantly reduced (even below 15%). This could cause problems in crashworthiness
468 of structures, e.g. in ship collision problems.

469 The presented results were subjected to significant scatter caused by the variability in mechanical
470 properties of intact specimens (due to inconsistencies in chemistries, processing temperatures, cooling
471 patterns, the strip thickness and numerous other factors [40]) and corrosion degradation. Thus, the
472 specimens of similar degradation levels were grouped for the analysis. In addition, the non-uniformity
473 of the corroded surfaces caused problems in the estimation of the elastic modulus. Particularly, the
474 typical mechanical extensometer that measures the elongation between two points was found to be
475 impractical. More advanced techniques, e.g. optical extensometer or Digital Image Correlation
476 equipment, seems to be needed for future studies to investigate the relationship between stress
477 distribution within specimen and degradation level. Further, the microstructure of corroded specimens
478 could be studied via X-ray micro tomography and adopted in FE model of corroded specimens. This
479 will allow to understand the relation between stresses and microstructure of corroded specimens.

480 It was found that although degradation level is easy to be measured in operating structure, it is not
481 that related to changes of mechanical properties with comparison to other parameters. Specifically,
482 the normalised area reduction factor, related to minimum cross-sectional area, was more correlated
483 with the drop of mechanical properties due to corrosion. However, this will require detail surface
484 recognition of corroded elements, with the use, e.g. 3-D scanning techniques or photogrammetry



485 measurements. This will require high working effort. Thus, future studies should look for other
486 governing parameters, particularly easily measured in a real structure or better diagnostic techniques
487 allowing to gather more information regarding corroded elements in less amount of time.

488 As the primary outcome of a presented analysis, the bilinear stress-strain relationships of corroded
489 steel were proposed together with uncertainty factors regarding the values of mechanical properties.
490 Such relationships can be used for fitness-for-purpose analyses in the structural integrity assessment
491 of corroded structures (including ships, offshore structures and onshore harbour facilities). For
492 example, this could be adopted in FE analysis of corroded structural elements, where degradation level
493 will be estimated based on the thickness measurements, and material will be modelled based on the
494 proposed relationships. However, in present study, thickness range between 5 mm up to 8 mm study
495 was investigated. The relationships for other thicknesses need to be studied in future, since higher
496 thicknesses are often used in marine structures.

497 **Acknowledgements**

498 This research was funded by The National Science Centre, Poland (grant No. 2018/31/N/ST8/02380,
499 entitled “Experimental and numerical investigations of progressive collapse of ageing structures
500 exposed to corrosion and locked cracks”).

501 **References**

- 502 [1] Melchers RE. Development of new applied models for steel corrosion in marine applications
503 including shipping. *Ships Offshore Struct* 2008;3:135–44.
- 504 [2] Guedes Soares C, Garbatov Y, Zayed A, Wang G. Corrosion wastage model for ship crude oil
505 tanks. *Corros Sci* 2008;50:3095–106.
- 506 [3] Bai Y, Jin W-L. Reassessment of Jacket Structure. *Mar. Struct. Des.*, Elsevier; 2016, p. 875–89.
- 507 [4] Woloszyk K, Kahsin M, Garbatov Y. Numerical assessment of ultimate strength of severe
508 corroded stiffened plates. *Eng Struct* 2018;168:346–54.
- 509 [5] Wang Y, Wharton JA, Sheno RA. Ultimate strength analysis of aged steel-plated structures
510 exposed to marine corrosion damage: A review. *Corros Sci* 2014;86:42–60.
- 511 [6] International Association of Classification Societies. Recommendation 87. Guidelines for
512 coating maintenance & repairs for ballast tanks and combined cargo/ballast tanks on oil
513 tankers. 2015.
- 514 [7] Garbatov Y, Guedes Soares C, Parunov J, Kodvanj J. Tensile strength assessment of corroded



- 515 small scale specimens. *Corros Sci* 2014;85:296–303.
- 516 [8] P. Domzalicki, I. Skalski, C. Guedes Soares YG. Large Scale Corrosion Tests. In: P.K. Das, editor.
517 *Anal. Des. Mar. Struct.*, Taylor & Francis Group; 2009, p. 193–8.
- 518 [9] Wang Y, Xu S, Wang H, Li A. Predicting the residual strength and deformability of corroded
519 steel plate based on the corrosion morphology. *Constr Build Mater* 2017;152:777–93.
- 520 [10] Nie B, Xu S, Yu J, Zhang H. Experimental investigation of mechanical properties of corroded
521 cold-formed steels. *J Constr Steel Res* 2019;162:105706.
- 522 [11] Qin G, Xu S, Yao D, Zhang Z. Study on the degradation of mechanical properties of corroded
523 steel plates based on surface topography. *J Constr Steel Res* 2016;125:205–17.
- 524 [12] Xu S, Zhang H, Wang Y. Estimation of the properties of corroded steel plates exposed to salt-
525 spray atmosphere. *Corros Eng Sci Technol* 2019;54:431–43.
- 526 [13] Xu S, Zhang Z, Li R, Wang H. Effect of cleaned corrosion surface topography on mechanical
527 properties of cold-formed thin-walled steel. *Constr Build Mater* 2019;222:1–14.
- 528 [14] Wu H, Lei H, Chen YF. Grey relational analysis of static tensile properties of structural steel
529 subjected to urban industrial atmospheric corrosion and accelerated corrosion. *Constr Build*
530 *Mater* 2021:125706.
- 531 [15] Jia C, Shao Y, Guo L, Liu Y. Mechanical properties of corroded high strength low alloy steel
532 plate. *J Constr Steel Res* 2020;172:106160.
- 533 [16] Kashani MM, Crewe AJ, Alexander NA. Nonlinear stress-strain behaviour of corrosion-
534 damaged reinforcing bars including inelastic buckling. *Eng Struct* 2013;48:417–29.
- 535 [17] Zhang W, Shang D, Gu X. Stress-strain relationship of corroded steel bars. *Tongji Daxue*
536 *Xuebao/Journal Tongji Univ* 2006;34.
- 537 [18] Fernandez I, Berrocal CG. Mechanical Properties of 30 Year-Old Naturally Corroded Steel
538 Reinforcing Bars. *Int J Concr Struct Mater* 2019;13:9.
- 539 [19] Li L, Mahmoodian M, Li CQ. Effect of corrosion on mechanical properties of steel bridge
540 elements. 9th Int. Conf. Bridg. MAINTENANCE, Saf. Manag., 2018.
- 541 [20] Li L, Li C-Q, Mahmoodian M. Effect of Applied Stress on Corrosion and Mechanical Properties
542 of Mild Steel. *J Mater Civ Eng* 2019;31:04018375.
- 543 [21] Ren C, Wang H, Huang Y, Yu Q-Q. Post-fire mechanical properties of corroded grade D36



- 544 marine steel. *Constr Build Mater* 2020;263:120120.
- 545 [22] Franceschini L, Vecchi F, Tondolo F, Belletti B, Sánchez Montero J. Mechanical behaviour of
546 corroded strands under chloride attack: A new constitutive law. *Constr Build Mater*
547 2022;316:125872.
- 548 [23] Du YG, Clark LA, Chan AHC. Residual capacity of corroded reinforcing bars. *Mag Concr Res*
549 2005;57:135–47.
- 550 [24] Cairns J, Plizzari GA, Du Y, Law DW, Franzoni C. Mechanical properties of corrosion-damaged
551 reinforcement. *ACI Mater J* 2005;102:256–64.
- 552 [25] Du YG, Clark LA, Chan AHC. Effect of corrosion on ductility of reinforcing bars. *Mag Concr Res*
553 2005;57:407–19.
- 554 [26] Palsson R, Mirza MS. Mechanical response of corroded steel reinforcement of abandoned
555 concrete bridge. *ACI Struct J* 2002;99:157–62.
- 556 [27] Garbatov Y, Saad-Eldeen S, Guedes Soares C, Parunov J, Kodvanj J. Tensile test analysis of
557 corroded cleaned aged steel specimens. *Corros Eng Sci Technol* 2018:1–9.
- 558 [28] Woloszyk K, Garbatov Y. Random field modelling of mechanical behaviour of corroded thin
559 steel plate specimens. *Eng Struct* 2020;212:110544.
- 560 [29] Woloszyk K, Garbatov Y. An enhanced method in predicting tensile behaviour of corroded
561 thick steel plate specimens by using random field approach. *Ocean Eng* 2020;213:107803.
- 562 [30] Moreno E, Cobo A, Palomo G, González MN. Mathematical models to predict the mechanical
563 behavior of reinforcements depending on their degree of corrosion and the diameter of the
564 rebars. *Constr Build Mater* 2014;61:156–63.
- 565 [31] Fernandez I, Bairán JM, Marí AR. Mechanical model to evaluate steel reinforcement corrosion
566 effects on σ - ϵ and fatigue curves. Experimental calibration and validation. *Eng Struct*
567 2016;118:320–33.
- 568 [32] Li D, Xiong C, Huang T, Wei R, Han N, Xing F. A simplified constitutive model for corroded steel
569 bars. *Constr Build Mater* 2018;186:11–9.
- 570 [33] Xiao L, Peng J, Zhang J, Ma Y, Cai CS. Comparative assessment of mechanical properties of HPS
571 between electrochemical corrosion and spray corrosion. *Constr Build Mater*
572 2020;237:117735.



- 573 [34] Woloszyk K, Garbatov Y, Kowalski J. Indoor accelerated controlled corrosion degradation test
574 of small- and large-scale specimens. *Ocean Eng* 2021;241:110039.
- 575 [35] ISO. Metallic materials - Tensile testing - Part 1: Method of test at room temperature. Int
576 Stand ISO 6892-1 2009.
- 577 [36] Woloszyk K, Garbatov Y. Accelerated large scale test set-up design in natural corrosion marine
578 environment. In: Guedes Soares C, Santos TA, editors. *Dev. Marit. Technol. Eng.*, London: CRC
579 Press; 2021, p. 517–24.
- 580 [37] Woloszyk K, Garbatov Y. Reliability of corroded stiffened plate subjected to uniaxial
581 compressive loading. *Int J Marit Eng* 2020;162 (A4):421–30.
- 582 [38] Woloszyk K, Garbatov Y. Structural Reliability Assessment of Corroded Tanker Ship Based on
583 Experimentally Estimated Ultimate Strength. *Polish Marit Res* 2019;26:47–54.
- 584 [39] Kwesi Nutor R. Using the Hollomon Model to Predict Strain-Hardening in Metals. *Am J Mater*
585 *Synth Process* 2017;2:1–4.
- 586 [40] Bright GW, Kennedy JI, Robinson F, Evans M, Whittaker MT, Sullivan J, et al. Variability in the
587 mechanical properties and processing conditions of a High Strength Low Alloy steel. *Procedia*
588 *Eng* 2011;10:106–11.
- 589

